



2020 7th International Conference on Power and Energy Systems Engineering (CPESE 2020),
26–29 September 2020, Fukuoka, Japan

Investigation on the C₄F₇N/N₂ Plasmas by Thomson Scattering

Haodong Chang, Hao Sun*, Panxin He, Yanwei Nan, Fei Yang, Hantian Zhang

State Key Laboratory of Electrical Insulation and Power Equipment, Xi'an Jiaotong University, Xi'an Shaanxi 710049, People's Republic of China

Abstract

Nowadays with the rapid development of the power system, the design of the power equipment should meet the demand of being eco-friendly. The serious greenhouse effect and long atmospheric lifetime of SF₆ limit its applications. As its alternative gas, heptafluoroisobutyronitrile (C₄F₇N) has been widely studied in recent years. Since the boiling temperature of C₄F₇N is high (-4.7 °C at 1 bar), N₂ or other gases with lower boiling temperature should be added for practical purposes. The goal of this work is to investigate the plasma behavior of C₄F₇N/N₂ mixtures. The plasma was created by focusing a Nd: YAG laser (1064 nm, 7 ns, 200 mJ) into a chamber filled with C₄F₇N/N₂ gas mixture at 1 bar. Another harmonic Nd: YAG laser (532 nm, 6 ns, 40 mJ) propagated in the radial direction of plasma, and then the radial distributions of electron density and temperature inside the plasma can be obtained by analyzing the Thomson scattering signal. When mixing more C₄F₇N molecules, the spatial range of the plasma tends to decrease, indicating the smaller size of plasma. The time-dependent electron density and temperature around the axis of the plasmas were fitted using the power law $A \cdot \Delta t^B$, and the decaying rate can be evaluated by the time exponent B . The time exponent of electron density decreases from -1.18 to -1.60 as the C₄F₇N ratio increases from 10% to 100%, indicating that the plasma decays more rapidly with higher C₄F₇N ratio. The electron temperature also shows the similar trend that the time exponent decreases from -0.68 in 10% C₄F₇N gas mixture to -1.34 in pure C₄F₇N gas. The decay of SF₆ plasma was investigated as a comparison and the time exponents of electron density and temperature are -1.52 and -0.69, respectively. In conclusion, as a potential substitute for SF₆, C₄F₇N/N₂ gas mixture has limited greenhouse effect and fast decaying process.

© 2020. Published by Elsevier Ltd.

Peer-review under responsibility of the scientific committee of the 7th International Conference on Power and Energy Systems Engineering (CPESE 2020).

Keywords: C₄F₇N; Thomson scattering; Electron density

* Corresponding author.

E-mail address: sunhao1031@xjtu.edu.cn (H. Sun).

© 2020. Published by Elsevier Ltd.

Peer-review under responsibility of the scientific committee of the 7th International Conference on Power and Energy Systems Engineering (CPESE 2020).

1. Introduction

Because of excellent arc quenching and insulation performances, sulphur hexafluoride (SF_6) has been used in gas insulated equipment (GIE), such as gas insulated switchgear (GIS). About 80% of production is consumed in power industry, and the consumption exceeds 10,000 tons [1]. However, the global warming potential (GWP) of SF_6 is 23,500 [2], leading to a serious greenhouse effect. To reduce the consumption, it is necessary to find an alternative. SF_6/N_2 mixture was firstly considered, but its dielectric strength is relatively low. Some perfluorocarbons (PFCs) have high dielectric strength, but the GWPs are typically between 5,000 and 12,000 [2]. In 2016, Minnesota Mining and Manufacturing (3MTM) and General Electric (GETM) announced an environmentally friendly gas mixture g^3 which is a compound of heptafluoroisobutryonitrile ($\text{C}_4\text{F}_7\text{N}$) and CO_2 . The insulation performance of $\text{C}_4\text{F}_7\text{N}$ is two times that of SF_6 and its GWP is 2,100 [2]. Besides, the chemical structure is easily destroyed in the atmosphere.

Some researchers have studied chemical and physical characteristics of $\text{C}_4\text{F}_7\text{N}$. Considering both local thermodynamic equilibrium (LTE) and nonlocal chemical equilibrium (LCE), Chen et al. [3] simulated $\text{C}_4\text{F}_7\text{N}$ arc plasma, and a detailed chemical kinetics model including the ionization, adsorption, excitation, and ion conversion reactions was helpful to understand arc plasmas. The insulation and decomposition characteristics of $\text{C}_4\text{F}_7\text{N}/\text{N}_2$ gas mixture were studied by Li et al. [4], and the mixture showed great self-recovery performance. Zhong et al. calculated the plasma properties of $\text{C}_4\text{F}_7\text{N}/\text{N}_2$ mixtures including equilibrium compositions, transport coefficients, thermodynamic properties and net emission coefficients [5]. Li et al. carried out acute toxicity tests and assessed the application risk of $\text{C}_4\text{F}_7\text{N}$. However, there is little experimental research on the microscopic parameters of $\text{C}_4\text{F}_7\text{N}$ plasma, especially the electron density and electron temperature.

In this work, the $\text{C}_4\text{F}_7\text{N}$ plasma was created by focusing a high-energy laser, which is known as laser-induced plasma (LIP). The method has been used in laser-triggered gas switch (LTGS) [6], laser-induced breakdown spectroscopy (LIBS) [7], etc. Another low-energy laser was applied to probe the $\text{C}_4\text{F}_7\text{N}$ plasma, and the electron density and temperature were obtained by collecting the Thomson scattering signal. Compared to optical emission spectroscopy (OES) methods, Thomson scattering does not assume that the plasma is axisymmetric and optically thin. Moreover, Thomson scattering has enough spatial-temporal resolution. Combining LIP and Thomson scattering, Zhang et al. [8] measured the electron density and temperature of air LIP. SF_6 plasmas at different pressures were investigated by Sun et al. [9] and SF_6 plasma has a special dynamics characteristic and fast decay. In this work, the electron density and temperature of $\text{C}_4\text{F}_7\text{N}/\text{N}_2$ plasma were measured spatially and temporally by Thomson scattering. As a promising substitute for SF_6 , the decay of $\text{C}_4\text{F}_7\text{N}/\text{N}_2$ plasma was compared with that of SF_6 plasma.

2. Experimental setup

The experimental setup is shown in Fig. 1. A Nd: YAG laser (1064 nm, 7 ns, 200 mJ) was focused by a 125 mm plano-convex lens to induce the plasma, which is called as the breakdown laser in this work. Another Nd: YAG laser (532 nm, 6 ns, 40 mJ) was loosely focused by a 250 mm plano-convex lens as the probe laser, and its fluence was below 20 J/cm². It should be pointed out that the plasma was disturbed by the probe laser. Mendys et al. [10] studied the heating effect of the probe laser and they summarized that the increase of electron temperature T_e was negligible if the fluence was lower than 20 J/cm² and the electron density n_e was less effected. Therefore, the energy of the probe was tuned to avoid obvious increase of T_e . A half-wave plate and a polarizing beam splitter compose an attenuator, and thus the continuous control of the laser energy can be achieved. Two lasers propagated through the glasses with high transmissivity in two perpendicular directions and the plasma was created and probed around the center of chamber. The chamber was firstly pumped to a pressure less than 0.5 Pa and then filled with $\text{C}_4\text{F}_7\text{N}$ and N_2 according to the settings of partial pressure ratios. The Thomson scattering was collected by a spectrometer and an ICCD in the direction perpendicular to two lasers. The signal with radially resolved resolution was achieved by rotating the plasma image onto the spectrometer slit. The two lasers and the ICCD were controlled by a digital delay generator (Stanford Research, DG535).

Thomson scattering [11] is the result of the interaction between low-energy photons and electrons. The electron density and temperature can be derived from the electron feature of the scattering signal. Thomson scattering can be evaluated by the scattering parameter α [8]:

$$\alpha = \frac{\lambda_0}{4\pi \sin(\theta/2)} \sqrt{\frac{4\pi n_e e^2}{\varepsilon_0 k_B T_e}} \quad (1)$$

where θ is the angle between the probe laser and the collection direction, λ_0 is 532 nm, n_e is the electron density, T_e is the electron temperature, k_B is the Boltzmann's constant, e is the charge of an electron and ε_0 is the permittivity in vacuum. When $\alpha > 1$, the scattering is in the collective regime and it can be simulated using the Salpeter approximation [12]. When $\alpha < 1$ (non-collective), an absolute calibration is additionally needed. In this work, the plasma is mainly in the collective regime.

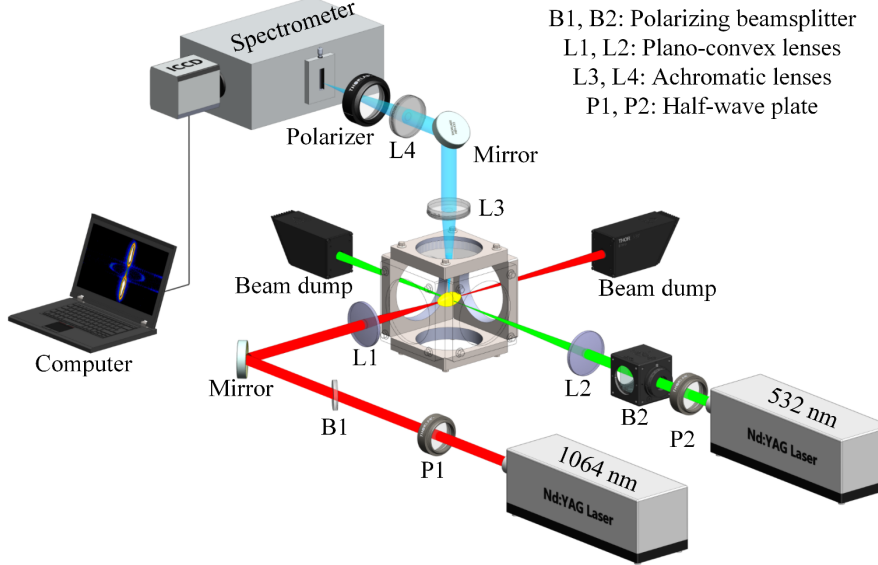


Fig. 1. Experimental setup.

3. Results and discussion

Fig. 2. (a) shows a radially resolved spectrum of 50%C₄F₇N/50%N₂ plasma at 2000 ns after the initial breakdown. The horizontal axis represents the wavelength while the vertical axis represents the radial direction of the plasma. It should be noted that the wavelength in the range from 531 nm to 533 nm includes strong Rayleigh scattering and stray light, and this range is excluded during the data processing. The Rayleigh scattering becomes stronger outside the plasma region. Thomson scattering appears as two sidebands which are symmetrically located around 532 nm. Because the probe laser propagated in the radial direction of the plasmas and the core of plasmas has the largest electron density and temperature, the scattering signal at $r = 0$ mm is the furthest from 532 nm. Apart from the broad

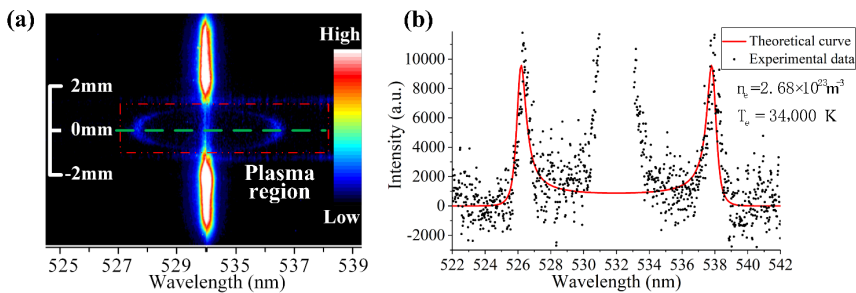


Fig. 2. Thomson scattering spectra: (a) a typical radially resolved spectrum; (b) the spectral data along the line marked by the green dashed line in Fig. 2. (a).

electron feature of Thomson scattering, Raman spectra can also be obviously seen at the edge of the plasma. The similar observation was also reported by Dzierżęga et al. [13], and the numerous Raman lines were located inside the plasma plume and outside the plasma region.

The detailed spectral data at $r = 0$ mm in Fig. 2. (a) is shown in Fig. 2. (b). The horizontal axis and vertical axis are the wavelength and spectral intensity, respectively. The red line is the theoretical curve of Thomson scattering, which is determined by different values of the electron density and temperature. The black points are spectral data, and the upward trend near 532 nm corresponds to the strong Rayleigh scattering, while the fluctuation in the wavelength range away from two sidebands (<524 nm, >540 nm) may correspond to the laser-induced breakdown spectroscopy (LIBS) of $\text{C}_4\text{F}_7\text{N}/\text{N}_2$ gas mixture. The theoretical curve fits well with the experimental data, and the electron density n_e and temperature T_e in this case are $2.68 \times 10^{23} \text{ m}^{-3}$ and 34,000 K, respectively.

Radial distributions of the electron density and electron temperature in different plasmas at various delays are shown in Fig. 3. The temporal resolution of plasmas can be achieved by changing the delay between the two lasers. At 1.5 μs , the central electron density of 50% $\text{C}_4\text{F}_7\text{N}$ plasma is slightly lower than that of 10% $\text{C}_4\text{F}_7\text{N}$ plasma, while the marginal electron density of 50% $\text{C}_4\text{F}_7\text{N}$ plasma, especially on the right side, is significantly lower than that of 10% $\text{C}_4\text{F}_7\text{N}$ plasma. This leads to a sharp gradient of electron density in 50% $\text{C}_4\text{F}_7\text{N}$ plasma. Subsequently, the 50% $\text{C}_4\text{F}_7\text{N}$ plasma shows a fast decay, and the central electron density decreases from $3.98 \times 10^{23} \text{ m}^{-3}$ at 1.5 μs to $5.06 \times 10^{22} \text{ m}^{-3}$ at 5.5 μs . In contrast, the central electron density of 10% $\text{C}_4\text{F}_7\text{N}$ plasma decreases from $4.18 \times 10^{23} \text{ m}^{-3}$ at 1.5 μs to $9.43 \times 10^{22} \text{ m}^{-3}$ at 5.5 μs . On the other hand, the symmetry of the distribution in 10% $\text{C}_4\text{F}_7\text{N}$ is disturbed at 1.5 μs , but there are good symmetric distributions of electron density at 3.5 μs and 5.5 μs . The distributions of electron density in 50% $\text{C}_4\text{F}_7\text{N}$ keeps asymmetric at three moments, and compared to the distribution at 1.5 μs , the asymmetry seems to exacerbate at 3.5 μs . This may be due to the non-uniform energy deposition of the breakdown laser [14], and more $\text{C}_4\text{F}_7\text{N}$ molecules exacerbate the asymmetry.

The distribution of electron temperature is more even compared to that of electron density. The similar distribution can also be found in the laser-induced plasmas of air [8]. Although the fluctuations of electron temperature exist in

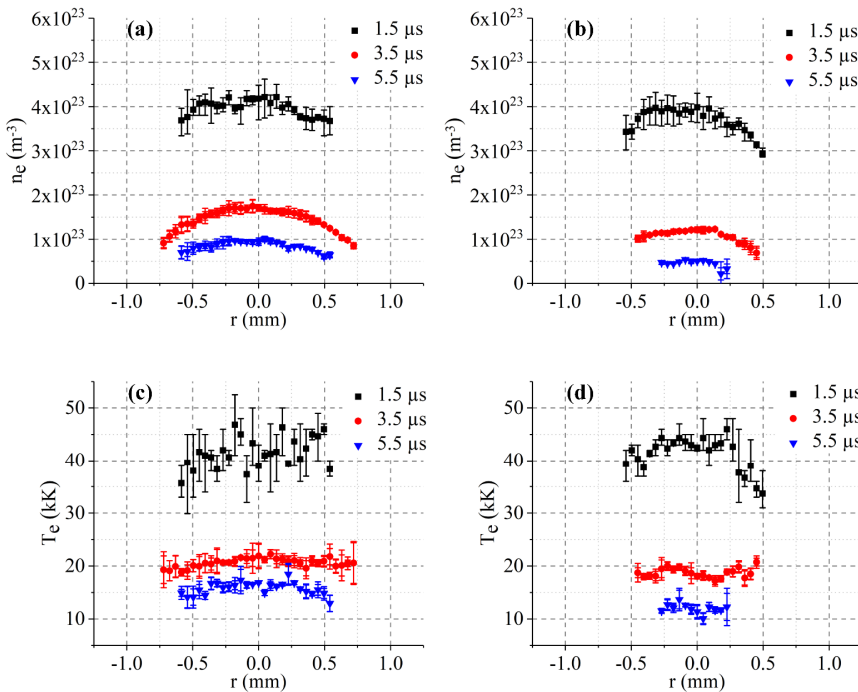


Fig. 3. Radial distributions of electron density and temperature of plasmas in different gas mixtures: (a) electron density n_e in 10% $\text{C}_4\text{F}_7\text{N}/90\%\text{N}_2$; (b) electron density n_e in 50% $\text{C}_4\text{F}_7\text{N}/50\%\text{N}_2$; (c) electron temperature T_e in 10% $\text{C}_4\text{F}_7\text{N}/90\%\text{N}_2$; (d) electron temperature T_e in 50% $\text{C}_4\text{F}_7\text{N}/50\%\text{N}_2$.

both 50% $\text{C}_4\text{F}_7\text{N}$ plasma and 10% $\text{C}_4\text{F}_7\text{N}$ plasma at 1.5 μs , values of electron temperature at all positions drop sharply after 2 μs , reaching a low value between 17,000 K and 22,000 K. After that, the decrease of electron temperature in 50% $\text{C}_4\text{F}_7\text{N}$ plasma is slightly faster than that in 10% $\text{C}_4\text{F}_7\text{N}$ plasma, indicating a faster decaying process with more $\text{C}_4\text{F}_7\text{N}$ molecules. It should be pointed out that the probe laser leads to an overestimation of the electron temperature although the laser energy has a low fluence.

The decaying process of plasmas in various gases is evaluated by fitting the data near the center (from $r = -0.045$ mm to $r = 0.045$ mm in Fig. 3.) with the power law $A \cdot \Delta t^B$ [8,15]. The time exponent, B , indicates the decaying rate of plasma and the smaller value of B implies the faster decaying rate. Temporal evolutions of n_e and T_e in certain gases are shown in Fig. 4. Meanwhile, the temporal evolutions of n_e and T_e in SF_6 plasma (1 bar) are also presented in Fig. 4. Detailed information about the time exponent is listed in Table 1. The Rayleigh scattering in pure $\text{C}_4\text{F}_7\text{N}$ plasma is extremely strong and the decay is fast, which limits the measurement in pure $\text{C}_4\text{F}_7\text{N}$ at both the early and late stage.

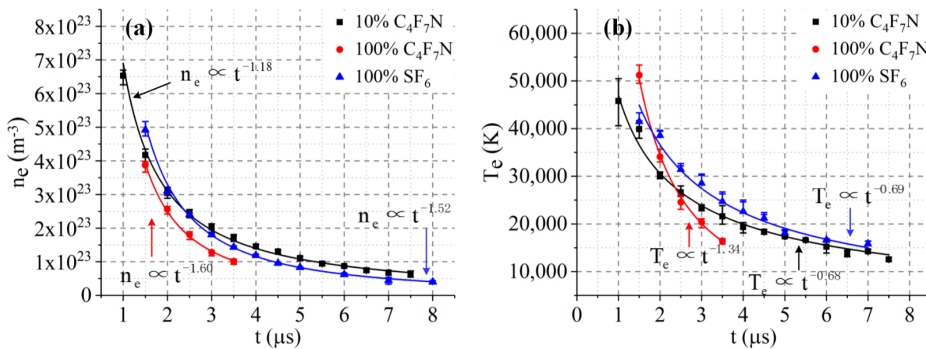


Fig. 4. Temporal evolution of (a) electron density and (b) electron temperature in different gases.

From 1.5 μs to 3.5 μs , the electron density in pure $\text{C}_4\text{F}_7\text{N}$ is always lower than that in pure SF_6 . The decay of electron density becomes faster as the ratio of $\text{C}_4\text{F}_7\text{N}$ increases, which is another reason for the superior arc quenching performance of $\text{C}_4\text{F}_7\text{N}$. The time exponent of electron density decreases from -1.18 to -1.60 with the ratio of $\text{C}_4\text{F}_7\text{N}$ increasing from 10% to 100%. Based on the same experimental platform and conditions, the decaying rate of electron density in SF_6 plasma is between 50% $\text{C}_4\text{F}_7\text{N}/50\%\text{N}_2$ and 100% $\text{C}_4\text{F}_7\text{N}$. This indicates that a proper ratio of $\text{C}_4\text{F}_7\text{N}/\text{N}_2$ gas mixture should be chosen for industrial applications. Zhong et al. [5] simulated the properties of arc plasmas, and they summarized that 50% could be the threshold of some characteristics of $\text{C}_4\text{F}_7\text{N}/\text{N}_2$ gas mixture. For example, the electrical conductivity of $\text{C}_4\text{F}_7\text{N}$ plasma mixtures will decrease remarkably if the proportion of the buffer gas is above 50%. The decay of electron temperature becomes faster with the increasing ratio of $\text{C}_4\text{F}_7\text{N}$ and it may be dominated by various processes such as three body recombination [10] and the hydrodynamic behaviours [8]. The difference between the electron temperatures in pure $\text{C}_4\text{F}_7\text{N}$ and those in pure SF_6 is quite large, which also proves the faster decay of $\text{C}_4\text{F}_7\text{N}$ plasma.

Table 1. Time exponents of the decay of electron density and temperature in various gases.

Gas	Time exponent of electron density	Time exponent of electron temperature
100% SF_6	-1.5182	-0.6869
10% $\text{C}_4\text{F}_7\text{N}/90\%\text{N}_2$	-1.1843	-0.6788
30% $\text{C}_4\text{F}_7\text{N}/70\%\text{N}_2$	-1.3605	-0.9044
50% $\text{C}_4\text{F}_7\text{N}/50\%\text{N}_2$	-1.4787	-1.0119
100% $\text{C}_4\text{F}_7\text{N}$	-1.5980	-1.3352

4. Conclusions

The radial distributions and decays of electron density and temperature in C₄F₇N/N₂ plasmas have been investigated. It is found that higher C₄F₇N ratio exacerbates the asymmetry of the energy deposition in plasma, leading to the asymmetric distributions of electron density. The distribution of electron temperature is more even compared to that of electron density. In addition, the power law was used to fit the time-dependent electron density and temperature at the center of different delays. The decay of plasmas gets faster with high C₄F₇N ratio. As the mixing ratio of C₄F₇N increases from 10% to 100%, the time exponent of electron density decreases from -1.18 to -1.60 while the time exponent of electron temperature decreases from -0.68 to -1.34. A comparison between the plasmas in C₄F₇N/N₂ mixture and pure SF₆ indicates that the electron density and temperature in C₄F₇N are lower than those in SF₆ after 2 μs, besides, the plasma in C₄F₇N has a faster decaying process. A further research and selection on the mixing ratio of C₄F₇N/N₂ is necessary for the practical applications.

Acknowledgements

This work was supported by National Natural Science Foundation of China (Nos. 51707144, 51877165), the Key Research and Development Program of Shaanxi Province (No. 2018ZDXMGY-112), the Research Program of Shaanxi Province (No. 2018KJXX-035 and No. 2019ZDLGY18-05) and State Key Laboratory of Electrical Insulation and Power Equipment (No. EIPPE19302).

References

- [1] M. Rabie and C. M. Franck. (2018) "Assessment of Eco-friendly Gases for Electrical Insulation to Replace the Most Potent Industrial Greenhouse Gas SF₆." *Environmental Science & Technology* 52.2 (2018): 369-380.
- [2] Y. Kieffel, T. Irwin, P. Ponchon, and J. Owens. (2016) "Green Gas to Replace SF₆ in Electrical Grids." *IEEE Power & Energy Magazine* 14.2 (2016): 32-39.
- [3] L. Chen, B. Zhang, J. Xiong, X. Li, and A. B. Murphy. (2019) "Decomposition mechanism and kinetics of iso-C4 perfluoronitrile (C₄F₇N) plasmas." *Journal of Applied Physics* 126.16 (2019): 163303.
- [4] Y. Li, X. Zhang, S. Xiao, Q. Chen, J. Tang, D. Chen, and D. Wang. (2018) "Decomposition Properties of C₄F₇N/N₂ Gas Mixture: An Environmentally Friendly Gas to Replace SF₆." *Industrial & Engineering Chemistry Research* 57.14 (2018): 5173-5182.
- [5] L. Zhong, J. Wang, J. Xu, X. Wang, and M. Rong. (2019) "Effects of Buffer Gases on Plasma Properties and Arc Decaying Characteristics of C₄F₇N-N₂ and C₄F₇N-CO₂ Arc Plasmas." *Plasma Chemistry and Plasma Processing* 39.3 (2019).
- [6] W. R. Rapoport, J. Goldhar, and J. R. Murray. (1980) "KrF Laser-Triggered SF₆ Spark Gap for Low Jitter Timing." *IEEE Transactions on Plasma Science* 8.3 (1980): 167-170.
- [7] D. W. Hahn and N. Omenetto. (2010) "Laser-Induced Breakdown Spectroscopy (LIBS), Part I: Review of Basic Diagnostics and Plasma-Particle Interactions: Still-Challenging Issues Within the Analytical Plasma Community." *Applied Spectroscopy* 64.12 (2010): 335.
- [8] H. Zhang, Y. Wu, H. Sun, F. Yang, M. Rong, and F. Jiang. (2019) "Investigations of laser-induced plasma in air by Thomson and Rayleigh scattering." *Spectrochimica Acta Part B: Atomic Spectroscopy* 157 (2019): 6-11.
- [9] H. Sun, H. Chang, M. Rong, Y. Wu, and H. Zhang. (2020) "Investigation of laser-induced plasma in SF₆ at different pressures using Thomson scattering." *Physics of Plasmas* 27.7 (2020): 073508.
- [10] A. Mendys, K. Dzierżęga, M. Grabiec, S. Pellerin, B. Pokrzywka, G. Travaille, and B. Bousquet. (2011) "Investigations of laser-induced plasma in argon by Thomson scattering." *Spectrochimica Acta Part B: Atomic Spectroscopy* 66.9 (2011): 691-697.
- [11] D. E. Evans and J. Katzenstein. (1969) "Laser light scattering in laboratory plasmas." *Reports on Progress in Physics* 32.1 (1969): 207-271.
- [12] E. E. Salpeter. (1960) "Electron Density Fluctuations in a Plasma." *Physical Review* 120.5 (1960): 1528-1535.
- [13] K. Dzierżęga, A. Mendys, and B. Pokrzywka. (2014) "What can we learn about laser-induced plasmas from Thomson scattering experiments." *Spectrochimica Acta Part B: Atomic Spectroscopy* 98 (2014): 76-86.
- [14] E. Nedanovska, G. Nersisyan, T. J. Morgan, L. Huwel, T. Murakami, C. Lewis, D. Riley, and W. G. Graham. (2015) "Investigating the dynamics of laser induced sparks in atmospheric helium using Rayleigh and Thomson scattering." *Journal of Applied Physics* 117.1 (2015): 013302.
- [15] A. Mendys, M. Kanski, A. Farahsougueh, S. Pellerin, B. Pokrzywka, and K. Dzierżęga. (2014) "Investigation of the local thermodynamic equilibrium of laser-induced aluminum plasma by Thomson scattering technique." *Spectrochimica Acta Part B: Atomic Spectroscopy* 96 (2014): 61-68.